Supplementary Information
Effects of 3D Geometries on Cellular Gradient Sensing and Polarization

Fabian Spill[1,2], Vivi Andasari[1], Michael Mak[1,2],
Roger D. Kamm[2,*], Muhammad H. Zaman[1,3,*]

June 6, 2016

[1]Department of Biomedical Engineering, Boston University, 44 Cummington Street, Boston MA 02215, USA.
[2]Department of Mechanical Engineering, Massachusetts Institute of Technology, 77 Massachusetts Avenue, Cambridge, MA 02139, USA.
[3]Howard Hughes Medical Institute, Boston University, Boston, MA 02215, USA.
[*] Co-corresponding authors, rdkamm@mit.edu (RDK), zaman@bu.edu (MHZ)

S1 Derivation and Consistency of the Membrane Binding-Unbinding Model

We model a molecule which is diffusing in a cell, can bind to and unbind from the cell membrane, and diffuse on the membrane when bound. Let G_c be the concentration of this molecule in the cytosol, i.e. the inside of a cell. We denote the domain of the cytosol by $V \subset \mathbb{R}^3$, which is a smooth Riemannian manifold with the metric induced from the Euclidean metric in $\mathbb{R}^3$. Likewise, G_m is the concentration of the same molecule when bound to the membrane, which is defined as the boundary of V, $S = \partial V$, and is an orientable Riemannian manifold. The membrane-bound molecules can unbind, and the molecules in the cytosol can bind to the membrane, with rates k_{on} and k_{off}, and where L_I is a length scale associated with the binding

range of a sequestered molecule to the membrane. Furthermore, D_M and D_C denote the diffusion coefficients for diffusion on the membrane and in the cytosol, respectively. Our equations are given by (1), which we repeat here for convenience:

$$\begin{aligned}
\frac{\partial \mathrm{G}_m(\bar{r}_m,t)}{\partial t} &= D_M \nabla_S^2 \mathrm{G}_m(\bar{r}_m,t) + k_{on} L_I \mathrm{G}_c(\bar{r}_m,t) - k_{off} \mathrm{G}_m(\bar{r}_m,t),\\
\frac{\partial \mathrm{G}_c(\bar{r}_c,t)}{\partial t} &= D_C \nabla_V^2 \mathrm{G}_c(\bar{r}_c,t),\\
-D_C e_n \nabla_V \mathrm{G}_c(\bar{r}_m,t) &= k_{on} L_I \mathrm{G}_c(\bar{r}_m,t) - k_{off} \mathrm{G}_m(\bar{r}_m,t),\\
\mathrm{G}_m(\bar{r}_m,0) &= \mathrm{G}_m^0(\bar{r}_m),\\
\mathrm{G}_c(\bar{r}_c,0) &= \mathrm{G}_c^0(\bar{r}_c).
\end{aligned} \tag{1}$$

Here, ∇_S^2, ∇_V^2 denote the Laplace operators (otherwise denoted as Laplacian, or Laplace-Beltrami operator) on S and V, respectively, and are defined in the usual way on Riemannian manifolds [1]. Furthermore, e_n denotes the uniquely defined unit outwards normal vector on the surface, and $\bar{r}_c \in V$, $\bar{r}_m \in S$. Hence, $e_n \nabla_V \mathrm{G}_c(\bar{r}_m,t)$ denotes the projection of the gradient of G_c on the unit normal vector on the surface. We have imposed the outwards normal flux in such a way that it matches the binding and unbinding reactions and preserves total particle numbers. Furthermore, $\mathrm{G}_m^0(\bar{r}_m), \mathrm{G}_c^0(\bar{r}_c)$ denote functions defining the initial conditions, and naturally G_m does not need any boundary conditions, as it is defined on a surface without boundary.

S1.1 Particle Number Conservation

We now show that the equations given in (1) conserve the number of particles. The total amount of molecules is given by

$$N = \int_V \mathrm{G}_c \, dV + \int_S \mathrm{G}_m \, dS. \tag{2}$$

This total amount of molecules is conserved by choice of boundary condition:

$$\begin{aligned}
\frac{\partial N}{\partial t} &= \int \frac{\partial \mathrm{G}_c}{\partial t} dV + \int \frac{\partial \mathrm{G}_m}{\partial t} dS \\
&= \int D_C div_V(grad_V \mathrm{G}_c) dV + \int (D_M div_S(grad_S \mathrm{G}_m) + k_{on} L_I \mathrm{G}_c - k_{off} \mathrm{G}_m) dS \\
&= \int D_C e_n (grad_V \mathrm{G}_c) dS + \int (D_M div_S(grad_S \mathrm{G}_m) + k_{on} L_I \mathrm{G}_c - k_{off} \mathrm{G}_m) dS \\
&= \int D_C e_n (grad_V \mathrm{G}_c) dS + \int (0 + k_{on} L_I \mathrm{G}_c - k_{off} \mathrm{G}_m) dS \\
&= \int (-k_{on} L_I \mathrm{G}_c + k_{off} \mathrm{G}_m + k_{on} L_I \mathrm{G}_c - k_{off} \mathrm{G}_m) dS \\
&= 0 \qquad (3)
\end{aligned}$$

In the first line of the derivation, we have simply plugged in the time derivatives of G_c and G_m from equation (1). Here, we have used that (on Riemannian manifold, independent of the coordinate system) we can write the Laplace operator as divergence of a gradient, where the subindices indicate the corresponding manifold in which divergence or gradient are calculated. We do not need the precise definition of gradient, divergence or Laplacian on those manifold, we only need the fact that the divergence theorem applies. Indeed, we apply the divergence theorem in the second step, changing from an integral of a divergence of the gradient of G_c over the whole cell to an integral of the normal flux over the boundary. Then, in the third step, we apply the divergence theorem to the divergence of the gradient of G_m. However, the surface does not have a boundary, so the divergence theorem immediately gives zero for this term. In the final step, we plug in the boundary condition from equation (1) for the normal flux of G_c at the boundary, and obtain our final result, that the total amount of particles is conserved.

S1.2 Global Invariance of Boundary Condition

Global conservation of particles is still ensured by adding a Laplacian of G_m to the flux boundary conditions:

$$-D_C e_n \nabla_V \mathrm{G}_c(\bar{r}_m, t) = k_{on} L_I \mathrm{G}_c(\bar{r}_m, t) - k_{off} \mathrm{G}_m(\bar{r}_m, t) + \lambda \nabla_S^2 \mathrm{G}_m(\bar{r}_m, t) \quad (4)$$

It is immediately clear that this preserves total particle numbers for any λ, for if we integrate the boundary condition over the whole boundary, this

term drops out by application of the divergence theorem over a manifold with empty boundary. However, for local conservation, we should not keep this term: If we choose $k_{on} = k_{off} = 0$, then m does not bind or unbind from the membrane at all and is conserved on its own (and not just the sum of bound and unbound molecules). However, keeping boundary condition (4) with $\lambda \neq 0$ would result in a flux of c even in that case. On physical grounds, we have to impose Neumann no-flux boundary conditions and the right-hand side of (4) should be zero. Hence, only $\lambda = 0$ ensures local conservation of particles.

S1.3 Derivation from a Model with Finite Binding Radius

We can consider a generalization of equations (1), (1) where the change of the membrane density $m(\bar{r}_m, t)$ is affected by all molecules in the cytosol within a finite radius L_I from the point $\bar{r}_m$. Then, the membrane binding-unbinding model is described by the equations

$$\begin{aligned}
\frac{\partial \mathrm{G}_m(\bar{r}_m, t)}{\partial t} &= D_M \nabla_S^2 \mathrm{G}_m(\bar{r}_m, t) \\
&\quad + \tilde{k}_{on} \int_{|\bar{r}_m - \bar{r}_c| \leq L_I} \mathrm{G}_c(\bar{r}_c, t) - k_{off} \mathrm{G}_m(\bar{r}_m, t) \\
\frac{\partial \mathrm{G}_c(\bar{r}_c, t)}{\partial t} &= D_C \nabla_V^2 \mathrm{G}_c(\bar{r}_c, t), \\
-D_C e_n \nabla_V \mathrm{G}_c(\bar{r}_m, t) &= \tilde{k}_{on} \int_{|\bar{r}_m - \bar{r}_c| \leq L_I} \mathrm{G}_c(\bar{r}_c, t) - k_{off} \mathrm{G}_m(\bar{r}_m, t). \qquad (5)
\end{aligned}$$

We have assumed that all molecules which are with a distance of L_I to a point on the membrane $\bar{r}_m$ are equally likely to be bound with a rate of $\tilde{k}_{on}$, which could be generalized further by including a kernel in the integral such that molecules closer to the membrane are more likely to bind. However, if we assume that L_I is small (see the discussion on parameters in the supplementary information S3.2) so that G_c does not significantly vary on this length scale, and that the membrane is not significantly curved on this scale, we can reduce the integral terms in (5). The integral will thus be over a half-sphere with radius L_I, so we can simplify $\tilde{k}_{on} \int_{|\bar{r}_m - \bar{r}_c| \leq L_I} \mathrm{G}_c(\bar{r}_c, t) = \tilde{k}_{on} \frac{1}{2} \frac{4}{3} \pi L_I^3 \mathrm{G}_c(\bar{r}_m, t) = k_{on} L_I \mathrm{G}_c(\bar{r}_m, t)$, where we have identified $k_{on} = \frac{2}{3} \pi L_I^2 \tilde{k}_{on}$. Hence, (5) reduces to equations (1), (1).

S1.4 Alternative Derivation from a Discrete Model

We now give an alternative derivation of equation (1) from a discrete model. We consider a small section of a cell near the cell membrane, so small that we can ignore the curvature of the membrane. Such section is shown in a schematic drawing on the right panel of Fig. S1, where the cell membrane is highlighted by the red surface. We are interested in the dynamics of the binding and unbinding of molecules to the membrane. Let L_I be the interaction length such that when a molecule in the cytosol is within a distance less or equal to L_I of the membrane, there is a probability of binding this molecule to the membrane. The associated binding rate is denoted by k_{on}. Likewise, unbinding is denoted k_{off}.

We define the domain of interest to be a cube of length $L \gg L_I$, which we discretize into equally spaced small cubes of size δ. Initially, we identify $\delta = L_I$. Each cube is labeled by integer-valued indices (k, l, p), and the membrane is located at the boundary $p = 0$. Then $M(k, l)$ denotes the number of membrane-bound molecules at the membrane segment adjacent to cube $(k, l, 0)$, and $C(k, l, p)$ denotes the number of cytosolic molecules in the cube (k, l, p). We consider the following processes: In the inner part of the cytosol, unbound molecules can diffuse only. At the cube adjacent to the membrane, they can diffuse in parallel to the membrane or away from the membrane, or they can bind to the membrane. On the other hand, membrane-bound molecules can unbind, or diffuse on the membrane. The following equations describe the rate of changes of the average number of molecules:

$$\begin{aligned}
\frac{\partial M(k,l)}{\partial t} &= \frac{D_M}{\delta^2}\left(M(k+1,l)+M(k-1,l)+M(k,l+1)+M(k,l-1)-4M(k,l)\right)+ \\
&\quad k_{on}C(k,l,0)-k_{off}M(k,l), \\
\frac{\partial C(k,l,p)}{\partial t} &= \frac{D_C}{\delta^2}(C(k+1,l,p)+C(k-1,l,p)+C(k,l+1,p)+C(k,l-1,p) \\
&\quad + C(k,l,p+1)+C(k,l,p-1)-6C(k,l)), \quad p>0, \\
\frac{\partial C(k,l,0)}{\partial t} &= \frac{D_C}{\delta^2}(C(k+1,l,0)+C(k-1,l,0)+C(k,l+1,0)+C(k,l-1,0) \\
&\quad + C(k,l,1)-5C(k,l))+k_{off}M(k,l)-k_{on}C(k,l,0)\,. \qquad (6)
\end{aligned}$$

We now want to study the continuum limit of those equations. First, we add

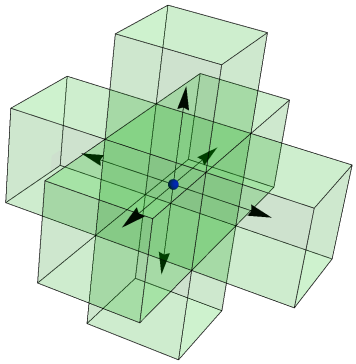

(a) Diffusion in cytosol

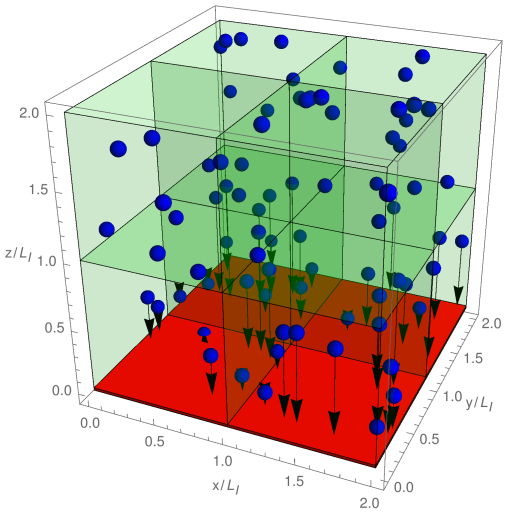

(b) Binding to the membrane

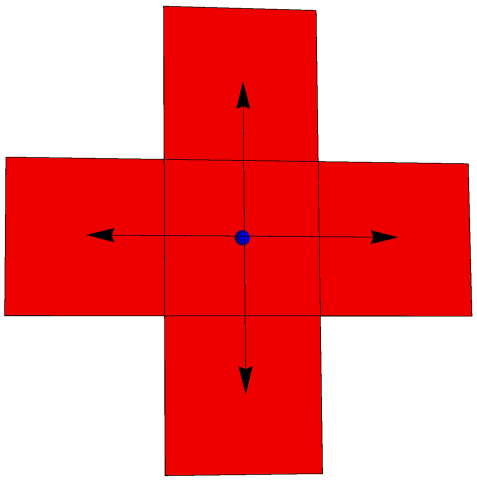

(c) Diffusion on membrane

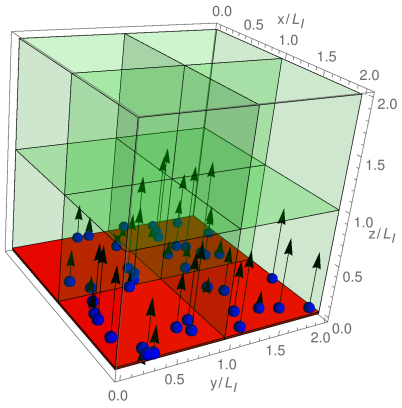

(d) Unbinding from the membrane

Figure S1: Molecules in the cytosol can move from their current cube to any of the nearest-neighbor cubes (figure (a)), or, if they are within a distance of the interaction range L_I to the membrane, they can bind to the membrane (figure (b)). Membrane-bound molecules can diffuse on the membrane only (figure(c)), or unbind from the membrane (figure (d)).

an artificial layer of cubes at $p = -1$, such that

$$C(k,l,-1) := \frac{\delta^2}{D_c}\left(k_{off}M(k,l) - k_{on}C(k,l,0)\right) + C(k,l,0)\,. \tag{7}$$

The benefit of this layer is that we can now combine the last two equations of (6) into

$$\begin{aligned}\frac{\partial C(k,l,p)}{\partial t} = \frac{D_C}{\delta^2}(&C(k+1,l,p) + C(k-1,l,p) + C(k,l+1,p) + C(k,l-1,p)\\ &+ C(k,l,p+1) + C(k,l,p-1) - 6C(k,l)), \quad p > -1\,,\end{aligned} \tag{8}$$

which is supplemented by (7). From those equations, it is straight-forward to take the continuum limit $\delta \to 0$. We define $\mathrm{G}_c(x,y,z) = \frac{C(k,l,p)}{\delta^3}$ to be the density of unbound molecules at a point (x,y,z), where we identify $(x,y,z) = (\delta k, \delta l, \delta p)$, and likewise $\mathrm{G}_m(x,y) = \frac{M(k,l)}{\delta^2}$ is the surface density of molecules bound to the membrane. Then, the continuum limit $\delta \to 0$ gives the following equation:

$$\begin{aligned}\frac{\partial \mathrm{G}_m(x,y)}{\partial t} &= D_M\nabla_S^2\mathrm{G}_m(x,y) + k_{on}\int_0^{L_I}\mathrm{G}_c(x,y,z)dz - k_{off}\mathrm{G}_m(x,y)\\ \frac{\partial \mathrm{G}_c(x,y,z)}{\partial t} &= D_C\nabla_V^2\mathrm{G}_c(x,y)\\ D_C\frac{\partial \mathrm{G}_c(x,y,0)}{\partial z} &= k_{on}\int_0^{L_I}\mathrm{G}_c(x,y,z)dz - k_{off}\mathrm{G}_m(x,y)\,.\end{aligned} \tag{9}$$

We have introduced the 2 and 3D surface or volume Laplace operators, ∇_S^2 and ∇_V^2, respectively. If we assume that the concentration in the cytosol does not vary much on a length scale of L_I, we can reduce these equations to the local model given by equation (1).

S1.5 Binding-Unbinding Equilibrium

We now consider the equilibrium condition between the binding and unbinding to and from the membrane, which is obtained from equation (3) by equating $L_I k_{on}\mathrm{G}_c = k_{off}\mathrm{G}_m$. The rates of binding and unbinding are set by k_{off} and $\frac{2k_{on}L_I}{R}$, respectively, where R is the cylinder radius. If f denotes the fraction of membrane-bound to total concentration,

$$f = \frac{\int_S \mathrm{G}_m dS}{\int_V \mathrm{G}_c dV + \int_S \mathrm{G}_m dS} \tag{10}$$

then, in a homogeneous equilibrium, we get

$$f = \frac{k_{on}}{k_{on} + k_{off}\frac{V}{L_I S}}, \tag{11}$$

as argued in the main text in equation (2).

S2 Dimensional Reduction of the 3D Model

We are now deriving the dimensional reduction of the 3D membrane binding/unbinding model (1).

S2.1 1D Reduction

We consider a cylindrical cell where the height of the cell is L and the radius is R, such that $L \gg R$. We choose cylindrical coordinates (r, ϕ, z) such that $r \in [0, R]$, $z \in [0, L]$ and cylindrical symmetry, so our fields G_m and G_c do not depend on $\phi \in [0, 2\pi]$. As G_m is the concentration of membrane bound molecules, it is only defined at the boundary of the cell located at $r = R$ and $z = 0, L$. Furthermore, the dependence of G_c on r is weak, relative to the dependence on z, due to fast radial diffusion due to $L \gg R$. We completely neglect the r dependence of G_m as this would only matter at $x = 0, L$, and would be weak, similar to the weakness of the r dependence of G_c.

The PDEs in cylindrical coordinates then become

$$\begin{aligned}
\frac{\partial \mathrm{G}_m(z,t)}{\partial t} &= D_M \partial_z^2 \mathrm{G}_m(z,t) + k_{on} L_I \mathrm{G}_c(R,z,t) - k_{off} \mathrm{G}_m(z,t) \\
\frac{\partial \mathrm{G}_c(r,z,t)}{\partial t} &= D_C \left(\partial_z^2 + \frac{1}{r} \partial_r r \partial_r \right) \mathrm{G}_c(r,z,t) \\
D_C \partial_r \mathrm{G}_c(R,z,t) &= -k_{on} L_I \mathrm{G}_c(R,z,t) + k_{off} \mathrm{G}_m(z,t), \\
D_C \partial_z \mathrm{G}_c(r,0,t) &= k_{on} L_I \mathrm{G}_c(r,0,t) - k_{off} \mathrm{G}_m(0,t), \\
D_C \partial_z \mathrm{G}_c(r,L,t) &= -k_{on} L_I \mathrm{G}_c(r,L,t) + k_{off} \mathrm{G}_m(L,t).
\end{aligned} \tag{12}$$

Then, let us define the following 1D densities

$$\begin{aligned}\tilde{\mathrm{G}}_c(z,t) &= \int_0^R \int_0^{2\pi} \mathrm{G}_c(r,z,t) r d\phi dr \\ &= 2\pi \int_0^R \mathrm{G}_c(r,z,t) r dr, \\ \tilde{\mathrm{G}}_m(z,t) &= \int_0^{2\pi} \mathrm{G}_m(z,t) R d\phi = 2\pi R \mathrm{G}_m(z,t). \end{aligned} \tag{13}$$

As R is assumed to be small such that diffusion in the radial direction is faster than other timescales in the problem, radial diffusion will quickly homogenize G_c in the radial direction even in the case when the initial conditions have a strong r dependence. Hence, ignoring potential fast transient changes of G_c, we consider G_c to have a weak dependence on r and expand $\tilde{\mathrm{G}}_c(z,t)$ to get

$$\begin{aligned}\tilde{\mathrm{G}}_c(z,t) &= 2\pi \int_0^R \left(\mathrm{G}_c(R,z,t) + \partial_r \mathrm{G}_c(R,z,t)(r-R) + \dots\right) r dr \\ &\approx 2\pi \left(\mathrm{G}_c(R,z,t)\frac{R^2}{2} - \frac{R^3}{6}\frac{1}{D_C}(k_{off}\mathrm{G}_m(z,t) - k_{on}L_I \mathrm{G}_c(R,z,t)) \right) \\ &= \pi R^2 \left(1 + \frac{RL_I}{3D_C}k_{on}\right) \mathrm{G}_c(R,z,t) - \frac{k_{off}R^2}{6D_C}\tilde{\mathrm{G}}_m(z,t). \end{aligned} \tag{14}$$

Here, we have expanded about $r = R$ and used the boundary condition. If we further assume that the radius R and the interaction range L_I are small such that the equation (6) holds, then we can approximate further (see section S3.2 for a discussion of those parameters)

$$\tilde{\mathrm{G}}_c(z,t) \approx \pi R^2 \mathrm{G}_c(R,z,t). \tag{15}$$

The 1D densities follow the differential equations

$$\begin{aligned}
\frac{\partial \tilde{\mathrm{G}}_m(z,t)}{\partial t} &= D_M \partial_z^2 \tilde{\mathrm{G}}_m(z,t) + 2\pi R k_{on} L_I \mathrm{G}_c(R,z,t)) - k_{off} \tilde{\mathrm{G}}_m(z,t), \\
&= D_M \partial_z^2 \tilde{\mathrm{G}}_m(z,t) + 2k_{on} \frac{L_I}{R} \tilde{\mathrm{G}}_c(z,t) - k_{off} \tilde{\mathrm{G}}_m(z,t), \\
\frac{\partial \tilde{\mathrm{G}}_c(z,t)}{\partial t} &= D_C \left(\partial_z^2 \tilde{\mathrm{G}}_c(z,t) + \int_0^R \left(\frac{1}{r} \partial_r r \partial_r \mathrm{G}_c(r,z,t) \right) 2\pi r dr \right), \\
&= D_C \left(\partial_z^2 \tilde{\mathrm{G}}_c(z,t) + 2\pi R \partial_r \mathrm{G}_c(R,z,t) \right), \\
&= D_C \left(\partial_z^2 \tilde{\mathrm{G}}_c(z,t) + 2\pi R \frac{1}{D_C} \left(k_{off} m(z,t) - k_{on} L_I \mathrm{G}_c(z,t) \right) \right), \\
&= D_C \partial_z^2 \tilde{\mathrm{G}}_c(z,t) + \left(k_{off} \tilde{\mathrm{G}}_m(z,t) - 2k_{on} \frac{L_I}{R} \tilde{\mathrm{G}}_c(z,t) \right),
\end{aligned} \tag{16}$$

which were given in the main text in equation (5). Mass conservation is ensured by accompanying those equations by Neumann no-flux boundary conditions. Note that while these equations are perfectly 1D PDEs, with the spatial domain defined by the length of the cylinder, the cylinder radius is still felt in the sense that the membrane-binding rate k_{on} is effectively renormalized by the inverse of the cylinder radius R.

S2.1.1 Equilibrium in One Spatial Dimensional

We consider the binding-unbinding equilibrium condition for the cylindrical cell in the 1D limit, as done in section S1.5 for a general 3D cell. We obtain for the fraction f of membrane-bound molecules

$$f = \frac{k_{on}}{k_{on} + k_{off} \frac{R}{2L_I}} = \frac{k_{on}}{k_{on} + k_{off} \sqrt{\frac{V}{4\pi L_I^2 L}}}, \tag{17}$$

as argued in equation (7). Notice that the dependence of f on V and L is different to the one found in [2], and we have checked that this difference is not because of the use of rectangular, rather than cylindrical cells. The binding/unbinding equilibrium and simultaneous 1D limit are valid if the

parameters satisfy the constraints

$$\frac{D_C}{R^2} \gg k_{off} \gg \frac{D_C}{L^2},$$
$$\frac{D_C}{R^2} \gg \frac{2k_{on}L_I}{R} \gg \frac{D_C}{L^2}. \tag{18}$$

These constraints ensure diffusion in the radial direction occurs on the fastest timescale to ensure there is only a weak radial dependence, and a 1D limit is justified. On the other hand, binding and unbinding are faster than diffusion along L so the binding/unbinding equilibrium is justified. We can then introduce an effective diffusion coefficient $D_{MC} = fD_M + (1-f)D_C$, similar as in [3, 2], so that the total concentration $G^{tot}(z,t) = \tilde{\mathrm{G}}_c(z,t) + \tilde{\mathrm{G}}_m(z,t)$ simply evolves by the standard 1D diffusion equation

$$\frac{\partial G^{tot}(z,t)}{\partial t} = D_{MC}\frac{\partial^2 G^{tot}(z,t)}{\partial z^2}. \tag{19}$$

We have thus reduced the original system of two coupled PDEs in three spatial dimensions to a single PDE in one spatial dimension. Note that other potential reactions in the system would need to be modified by f accordingly, and, if they are present, the timescales of associated with those reactions need to be compared to the timescales of radial diffusion and binding/unbinding to justify the reduction of the complete model with reactions to lower dimensions.

S2.2 2D Reduction

Let us consider a flat cell, which, for simplicity, we take to be a disk of radius R and height h. Hence, it is natural to choose cylindrical coordinates, and the full model is described by (12), with L replaced by h. We now consider the limit $h \ll R$. Then, we can rewrite the z-dependence of the Laplacian as

$$\begin{aligned} D_C\frac{\partial^2 \mathrm{G}_c(r,\phi,z,t)}{\partial_z^2} &\approx D_c\frac{\partial_z \mathrm{G}_c(r,\phi,h) - \partial_z \mathrm{G}_c(r,\phi,0)}{h}, \\ &= \frac{k_{off}}{h}\left(\mathrm{G}_m(r,h,t) + \mathrm{G}_m(r,0,t)\right) \\ &\quad - \frac{k_{on}L_I}{h}\left(\mathrm{G}_c(r,\phi,h,t) + \mathrm{G}_c(r,\phi,0,t)\right). \end{aligned} \tag{20}$$

If the concentrations only depend very weakly on z, then we can simplify the system by introducing

$$\begin{aligned}\hat{\mathrm{G}}_c(r,\phi,t) &= \int_0^h \mathrm{G}_c(r,\phi,z,t)dzdr = h\mathrm{G}_c(r,\phi,t),\\ \hat{\mathrm{G}}_m(r,\phi,t) &= 2\mathrm{G}_m(r,\phi,t),\end{aligned} \tag{21}$$

and get

$$\begin{aligned}\frac{\partial\hat{\mathrm{G}}_m(r,\phi,t)}{\partial t} &= D_M\nabla_P^2\hat{\mathrm{G}}_m(r,\phi,t) + 2k_{on}\frac{L_I}{h}\hat{\mathrm{G}}_c(r,\phi,t) - k_{off}\hat{\mathrm{G}}_m(r,\phi,t),\\ \frac{\partial\hat{\mathrm{G}}_c(r,\phi,t)}{\partial t} &= D_C\nabla_P^2\hat{\mathrm{G}}_c(r,\phi,t) - 2k_{on}\frac{L_I}{h}\hat{\mathrm{G}}_c(r,\phi,t) + k_{off}\hat{\mathrm{G}}_m(r,\phi,t).\end{aligned} \tag{22}$$

Here, ∇_P^2 denotes the conventional 2D Laplace operator in polar coordinates. Similarly to the 1D case, the scaling of the parameters is different. Similarly to the 1D case, we find that the parameters of the reduced geometry, in this case, the cylinder height h, renormalize the effective membrane-binding coefficient. As before, we consider the steady-state solution where f denotes the fraction of membrane-bound molecules. Hence, for the oblate cylinder we get

$$f = \frac{k_{on}}{k_{on} + k_{off}\frac{h}{2L_I}}. \tag{23}$$

S3 3D Polarization Pathway

In this section, we discuss in detail how our 3D pathway model discussed in section 2.2, is obtained and relates to the 1D model discussed in [2].

S3.1 Model Setup

The 1D model of [2] was motivated by experiments where cells were constrained in effective 1D geometries. It was assumed that the approximate 3D geometry is rectangular with length scales $L \gg w > d$, with an initial length of $L = 20\mu m$. The volume of a cell in the experimental paper [4], which uses the model of [2], was given as approximately $V = 800\mu m^3$. The supplementary information of [4] mentions $d = 0.2\mu m$, which seems a bit small for a real cell and would also imply that $w = 200\mu m$ at the given volume.

We hence compare to a cell with base measure $L, w, d = 20, 8, 5\mu m$. In [4], the cells were about $80\mu m$ long (see e.g. figure S4 in [4]), which would, at the same volume, be compatible with $L, w, d = 80, 5, 2\mu m$. Such cell seems also compatible with the 1D limit as described in the section 2.3 of the main text. In [2, 4] the change in cell length was taken into account by changing the fraction of membrane bound to unbound inactive molecules via an equation similar, but slightly different, to our equation (7). The 3D model will automatically take into account any geometry change. The basic equations for the evolution of the three GTPases now takes into account that the each GTPase can exist in an active, membrane bound form G_{ma}, a membrane bound, inactive form G_{mi} and a form G_c which diffuses inactively through the cytosol. These follow the principal scheme

$$\begin{aligned}
\frac{\partial \mathrm{G}_{ma}}{\partial t} &= D_M \nabla_S^2 \mathrm{G}_{ma} + I_G \mathrm{G}_{mi} - \delta_G \mathrm{G}_{ma}, \\
\frac{\partial \mathrm{G}_{mi}}{\partial t} &= D_M \nabla_S^2 \mathrm{G}_{mi} - I_G \mathrm{G}_{mi} + \delta_G \mathrm{G}_{ma} + k_{on} L_I \mathrm{G}_c - k_{off} \mathrm{G}_{mi}, \\
\frac{\partial \mathrm{G}_c}{\partial t} &= D_C \nabla_V^2 \mathrm{G}_c, \\
-D_C e_n \nabla_V \mathrm{G}_c &= k_{on} L_I \mathrm{G}_c - k_{off} \mathrm{G}_{mi}.
\end{aligned} \tag{24}$$

Here, I_G represents the activation, and δ_G the deactivation rate, whereas k_{on}, k_{off} denote the binding and unbinding rates as in the section 2. Note that equations (24) are slightly different from the equations given in the appendix of [2], which were used to motivate the 1D model from a 3D perspective.

We note that to account for the proper localization of the membrane bound and unbound species $\mathrm{G}_{ma}, \mathrm{G}_{mi}$ and G_c, we measure G_c in Molar, but $\mathrm{G}_{ma}, \mathrm{G}_{mi}$ in $\frac{mol}{m^2}$. Whereas this latter measure is not often chosen in experiments, as usually total cell concentrations are measured, this is nevertheless the physically more meaningful measure, as $\mathrm{G}_{ma}, \mathrm{G}_{mi}$ denote number molecules per two dimensional membrane area, and this choice ensures that our equations and the dimensional reductions have the correct units. To compare with [2], we will hence multiply the concentrations of active GTPases with $\frac{V_0}{S_0} = \frac{800\mu m^3}{600\mu m^2} = 4/3\mu m$, the fraction of volume to surface area for the above mentioned rectangular cell of basic length $L, w, d = 20, 8, 5\mu m$. With this setup, it is straight-forward to generalize the 1D model from [2], summarized in figure 1, in our 3D context, and one obtains equations (3). All coefficients apart from the membrane binding and unbinding rates are

taken from [2, 4], but those which multiply a membrane density are multiplied by the factor $\frac{V_0}{S_0}$. Furthermore, to compare the activation rates given in [2, 4] with ours we need to divide them with the fraction of bound to total inactive molecules f, as we separately consider bound and unbound inactive GTPases. We now summarize the use of the spatially dependent Rac stimulus S_{Rac} which appears in the activation rate for Rac, equation (4) in most simulations shown in section 3. If the x-axis denotes the direction of the stimulus, then typically we assumed a linear stimulus of strength $S_{Rac} = 0.5 I_{R1} \frac{x}{20\mu m}$, where I_{R1} is the baseline Rac activation rate as given in Table S1. The baseline length of $20\mu m$ is chosen to match results from earlier works, as described above. In figures 9, 10 and S3 such gradient was used but then rotated towards the indicated axis at $t = 100s$.

S3.2 Parameter Estimation

We now investigate when the use of the 1D model is justified for the case where the molecule is a small GTPase. We have $D_C = 100\mu m^2/s$ [3, 4]. Furthermore, we estimate that the interaction range of the binding reaction, L_I, approximately corresponds to the size of the molecules. We have a molecular weight of the small GTPases of about $21kDa$. Exact size determination of proteins is tricky [5], but here we only need a rough estimate, which gives that we have a volume of $V = \frac{21*1.6*10^{-27}kg}{1kg/l} = 3*10^{-26}m^3 = 30nm^3$. Hence, the interaction length scale is on the order of a few nanometers. We put $L_I = 2nm$, and this estimate is similar to stimations made in similar contexts [6]. Furthermore, we can safely assume that $R \gg L_I$ for realistic cell geometries. Then, unless $k_{on} \gg k_{off}$, of the two requirements $\frac{RL_I k_{on}}{3D_C} \ll 1$, $\frac{k_{off}R^2}{6D_C} \ll 1$, the first one automatically holds provided the second one does. From [7] we can estimate that k_{off} should be faster than $k_{off} = 0.06s^{-1}$, as the combined deactivation/unbinding rate (this combined rate is denoted k_{off} in [7]) is of this magnitude. However, the actual binding and unbinding rates are influenced by the presence of other regulators such as GDI molecules [8] and might be different for GTP and GDP bound GTPases, and is hence also influenced by the presence of GEFs and GAPs. Here, we focus on rough estimates and use the above numbers to derive a limit for the radial length scale of

$$R \ll \sqrt{\frac{6D_C}{k_{off}}} \leq \sqrt{\frac{600}{0.06}}\mu m = 100\mu m. \tag{25}$$

As long as k_{off} is not too large this condition is satisfied for realistic cell dimensions. However, if k_{off} should be significantly larger than estimated above then this limit might be hard to satisfy.

Now we look at the steady-state assumption between bound and unbound GTPase. For this, we have

$$L \gg \sqrt{\frac{D_C}{k_{off}}}. \tag{26}$$

With $k_{off} = 0.06s^{-1}$, we get $L \gg 30\mu m$ would safely satisfy this constraint. However, most likely k_{off} is significantly larger so the steady-state assumption is most likely valid for shorter cells as well.

All other parameters used in equations (3) are summarized in Table S1. Lacking accurate measurements of k_{off}, it is commonly believed that k_{off} is much faster larger than the deactivation rate [7, 2]. As the deactivation rates were estimated in [2] to be $1s^{-1}$, we take $k_{off} = 10s^{-1}$. While the total unbinding/deactivation rate was estimated in [7] to be much smaller than $1s^{-1}$, we stick to those values here as we first would like to compare our 3D model to the 1D model of [2]. In the subsection 3.2 in the main text we study the influence of varying k_{off} on the polarization behavior of the cell. We also need to determine the combination of parameters $k_{on}L_I$. From the estimates of D_C, D_M, combined with the estimate that at baseline length of $L = 20\mu m$ the diffusion coefficient for total inactive GTPases (bound and unbound) is $50\mu m^2/s$, we get that about half of the inactive GTPases molecules are typically membrane bound. This equilibrium value can then be used to deduce $k_{on}L_I$ via equation (2).

S3.3 Implementation of the 3D Model

All simulations of the 3D model were performed in COMSOL Multiphysics 5.1 (COMSOL, Inc, Burlington, MA) using the General PDE model framework. We remark that the default solver occasionally produced too large time steps, requiring us to manually limit the maximal time step depending on the model parameters. It is also necessary to choose a fine mesh for good spatial resolution in several cases, for instance, when the cytosolic species vary sharply at the membrane. In most cases, the predefined Mesh Element settings 'Finer' or 'Extra Fine' were sufficient to ensure spatial convergence.

Dimensional parameter	Estimate
D_C	100 μm^2 s^{-1}
D_M	1μm^2 s^{-1}
D_P	5μm^2 s^{-1}
$\mathrm{Rac}_{tot,2}$	10nmol m^{-2}
$\mathrm{Rho}_{tot,2}$	4nmol m^{-2}
$\mathrm{Cdc}_{tot,2}$	3.4nmol m^{-2}
P_{3b}	0.2nmol m^{-2}
δ_R	1s^{-1}
δ_ρ	1s^{-1}
δ_C	1s^{-1}
δ_{P_1}	0.21s^{-1}
k_{21}	0.021s^{-1}
$k_{\max}$	2.8s^{-1}
k_{P_2}	2.1s^{-1}
α	1.3s^{-1}
μ_P	0.011s^{-1}
G	0.03s^{-1}
I_{R1}	0.4μM s^{-1}
I_{R2}	0.4μM s^{-1}
I_{Rho}	13.2μMs^{-1}
I_{Cdc}	5.9μMs^{-1}
I_{P_1}	14nmol m^{-2} s^{-1}
a_1	1.7nmol m^{-2}
a_2	1.3nmol m^{-2}
k_{PI5K}	0.084s^{-1}
k_{PI3K}	0.00072s^{-1}
k_{PTEN}	0.432s^{-1}
f_1	1
k_{off}	10s^{-1}
$k_{on}L_I$	13.3μm s^{-1}

Table S1: Parameters of the cell polarization model equation (3), inferred for a cell with dimensions $L, w, d = 20, 8, 5\mu m$, so all values which multiply membrane concentrations are rescaled by the factor $\frac{V_0}{S_0} = \frac{4}{3}\mu m$. This means $1\mu M \frac{V_0}{S_0} = \frac{4}{3}\frac{nmol}{m^2}$. Furthermore, α, I_{R1}, I_{R2} I_{Rho} and I_{Cdc} are multiplied by the baseline fraction of bound inactive molecules f. We have also rounded the parameters as appropriate.

References

[1] Jürgen Jost. *Riemannian Geometry and Geometric Analysis*. Springer Science & Business Media, 2008.

[2] William R Holmes, Benjamin Lin, Andre Levchenko, and Leah Edelstein-Keshet. Modelling cell polarization driven by synthetic spatially graded rac activation. *PLoS Computational Biology*, 8(6):e1002366, 2012.

[3] Adriana T Dawes and Leah Edelstein-Keshet. Phosphoinositides and rho proteins spatially regulate actin polymerization to initiate and maintain directed movement in a one-dimensional model of a motile cell. *Biophysical Journal*, 92(3):744–768, 2007.

[4] Benjamin Lin, William R Holmes, C Joanne Wang, Tasuku Ueno, Andrew Harwell, Leah Edelstein-Keshet, Takanari Inoue, and Andre Levchenko. Synthetic spatially graded rac activation drives cell polarization and movement. *Proceedings of the National Academy of Sciences*, 109(52):E3668–E3677, 2012.

[5] Harold P Erickson. Size and shape of protein molecules at the nanometer level determined by sedimentation, gel filtration, and electron microscopy. *Biol Proced Online*, 11(1):32–51, 2009.

[6] Stuart McLaughlin and Alan Aderem. The myristoyl-electrostatic switch: a modulator of reversible protein-membrane interactions. *Trends in Biochemical Sciences*, 20(7):272–276, 1995.

[7] Konstadinos Moissoglu, Boris M Slepchenko, Nahum Meller, Alan F Horwitz, and Martin A Schwartz. In vivo dynamics of rac-membrane interactions. *Molecular Biology of the Cell*, 17(6):2770–2779, 2006.

[8] Athanassios Dovas and John Couchman. Rhogdi: multiple functions in the regulation of rho family gtpase activities. *Biochem. J*, 390:1–9, 2005.

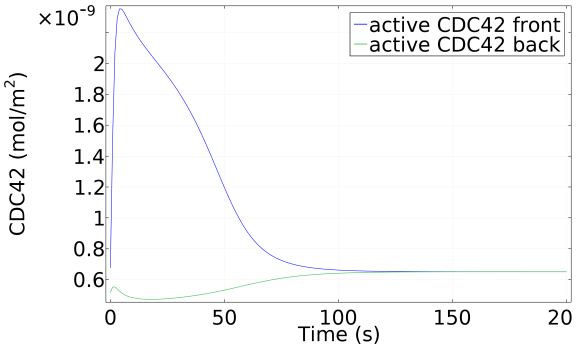

(a) $L = 20\mu m$

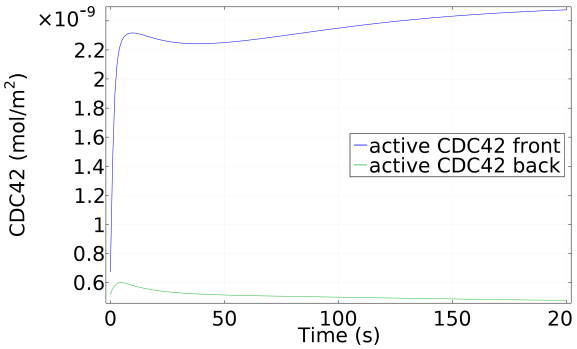

(b) $L = 40\mu m$

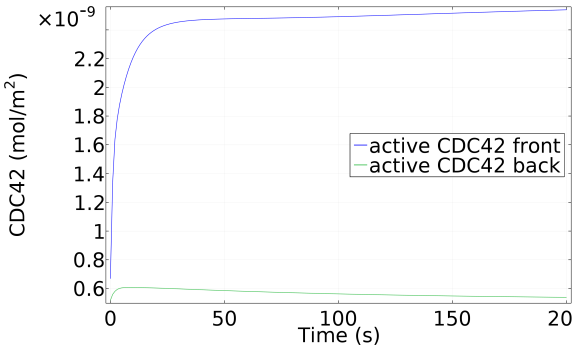

(c) $L = 80\mu m$

Figure S2: The time evolution of concentration of active Cdc42 in time at the front and back of the rectangular cells as shown in figures 2 and 3.

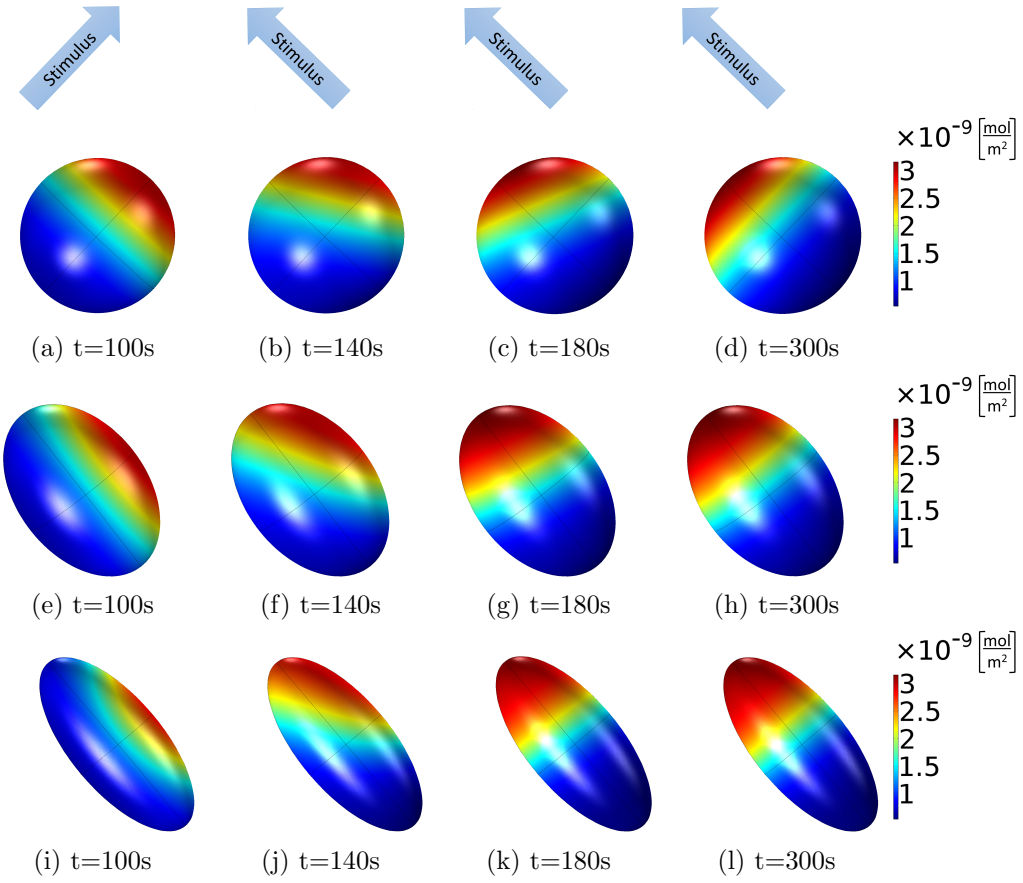

Figure S3: As in figures 9, 10, active Rac on the membrane is shown for different times and cells of different shapes, but here, the Rac activation rate in the first $100s$ increases linearly along a short axis of the ellipsoid (from lower left corner to upper right corner), and from then on, it increases linearly along the long axis of the ellipsoids (from the lower right corner to the upper left corner). In all cases, the volume of the ellipsoid cells is fixed as $V = 800\mu m^3$, the main axis is $11.5\mu m$ (spherical, (a)-(d)), $15\mu m$ ((e)-(h)) and $20\mu m$ ((i)-(l)), and the other two axes are of the same length. Cells of all shapes are able to adapt to their new stimulus direction, with the elongated cells being slightly faster.